Inorg. Chem. **2004**, *43*, 2049–2056

Synthesis, Crystal Structure, and Physical Properties of (BEDT-TTF)[Ni(tdas)$_2$] (BEDT-TTF = Bis(ethylenedithio)tetrathiafulvalene; tdas = 1,2,5-Thiadiazole-3,4-dithiolate): First Monomeric [Ni(tdas)$_2$]$^-$ Monoanion

S. Curreli,[†] P. Deplano,[‡] M. L. Mercuri,*[,‡] L. Pilia,[‡] A. Serpe,[‡] John A. Schlueter,*[,§] Michael A. Whited,[§] Urs Geiser,[§] E. Coronado,[†] C. J. Gómez-García,[†] and E. Canadell[||]

Instituto de Ciencia Molecular, Universidad de Valencia, Dr. Moliner 50, E-46100, Burjasot, Spain, Dipartimento di Chimica Inorganica ed Analitica, SS 554, Bivio per Sestu, I09042 Monserrato (Cagliari), Italy, Materials Science Division, Argonne National Laboratory, Argonne, Illinois 60439-4831, and Institut de Ciència de Materials de Barcelona (CSIC), Campus de la UAB, 08193 Bellaterra, Spain

Received September 11, 2003

We report the synthesis, structure, and physical properties of (BEDT-TTF)[Ni(tdas)$_2$] [BEDT-TTF, or ET, is bis(ethylenedithio)tetrathiafulvalene; tdas is 1,2,5-thiadiazole-3,4-dithiolate], which is the first example of a salt containing monomeric [Ni(tdas)$_2$]$^-$ monoanions. This salt, which crystallizes in the monoclinic space group $P2_1/c$ with a = 17.2324(6) Å, b = 13.2740(5) Å, c = 10.9467(4) Å, β = 96.974(2)°, and V = 2485.5(2) Å^3, forms a layered structure. One layer contains dimerized BEDT-TTF electron donor molecules and isolated [Ni(tdas)$_2$]$^-$ monoanions, while the second layer contains chains of [Ni(tdas)$_2$]$^-$ monoanions. Conductivity measurements show that (BEDT-TTF)[Ni(tdas)$_2$] has a semiconductor-to-semiconductor transition near 200 K, while magnetic measurements indicate that it is an S = 1/2 paramagnet with weak antiferromagnetic coupling. Reflectance spectra reveal bands in the near-infrared region (6.6×10^3 and 10.6×10^3 cm^{-1}) which are typical of (BEDT-TTF)$_2^{2+}$ dimers. From these data, we can conclude that the unpaired electron lies on the [Ni(tdas)$_2$]$^-$ anions. Tight-binding band structure calculations were used to analyze the electronic structure of this salt.

Introduction

Metal bis(dithiolene) complexes are of special interest in material chemistry because of their ability to form single-component molecular metals[1] in addition to superconducting[2,3] and ferromagnetic[4] salts.[5] Among them, metal complexes of the ligand 1,2,5-thiadiazole-3,4-dithiole (tdas) were prepared one decade ago as potential analogues of the [M(dmit)$_2$]$^{x-}$ systems (dmit = 2-thioxo-1,3-dithiole-4,5-dithiolate, M = Ni, Pd; $0 < x < 2$). In particular, the tdas compounds are much easier to obtain in a one-step reaction from commercial precursors than the dmit-based complexes. Furthermore, the iron salt TBA[Fe(tdas)$_2$] (TBA = tetrabutylammonium),[6] which exhibits a dimeric structure and magnetic properties typical of an antiferromagnetic dimer, shows two unusual phase transitions in the 190−240 K range. These transitions have been explained as reentrant phase behavior, where the low- and high-temperature phase are identical while a second phase with a different value of the antiferromagnetic exchange coupling constant exists at intermediate temperatures.

These tdas systems are therefore attractive as components of multifunctional molecular solids where an interplay or a coexistence of two physical properties may be found. A TTF

* To whom correspondence should be addressed. E-mail: mercuri@unica.it (M.L.M.); JASchlueter@anl.gov (J.A.S.).
[†] Universidad de Valencia. E-mail: eugenio.coronado@uv.es (E.C.).
[‡] Dipartimento di Chimica Inorganica ed Analitica.
[§] Argonne National Laboratory.
[||] Institut de Ciència de Materials de Barcelona (CSIC).

(1) Tanaka, H.; Okano, Y.; Kobayashi, H.; Suzuki, W.; Kobayashi, A. *Science* **2001**, *291*, 285.
(2) Tajima, H.; Inokuchi, M.; Kobayashi, A.; Ohta, T.; Kato, R.; Kobayashi, H.; Kuroda, H. *Chem. Lett.* **1993**, 1235.
(3) Cassoux, P.; Valade, L. In *Inorganic Materials*, 2nd ed.; Bruce, D. W., O'Hare, D., Eds.; John Wiley & Sons: Chichester, U.K., 1996; p 1.
(4) Coomber, A. T.; Beljonne, D.; Friend, R. H.; Brédas, J. L.; Charlton, A.; Robertson, N.; Underhill, A. E.; Kurmoo, M.; Day, P. *Nature (London)* **1996**, *380*, 144.
(5) Robertson, N.; Cronin, L. *Coord. Chem. Rev.* **2002**, *227*, 93.
(6) Awaga, K.; Okuno, T.; Maruyama, Y.; Kobayashi, A.; Kobayashi, H.; Schenk, S.; Underhill, A. E. *Inorg. Chem.* **1994**, *33*, 5598.

10.1021/ic035079y CCC: $27.50
Published on Web 02/17/2004

(TTF = tetrathiafulvalene) salt of the $[Fe(tdas)_2]^-$ anion has been previously prepared and characterized.[7] The crystal structure and magnetic susceptibility of $(TTF)_2[Fe(tdas)_2]$ indicated that this structure possesses antiferromagnetic $[Fe(tdas)_2]_2^{2-}$ dimers and a coexistence of delocalized and localized unpaired electrons. An anomaly was observed in the magnetic susceptibility between 80 and 96 K, but no evidence for a reentrant transition was present. Very recently, after many attempts, we obtained by electrocrystallization methods crystals suitable for a structural characterization of $(BEDT\text{-}TTF)_2[Fe(tdas)_2]$ [BEDT-TTF, or ET, is bis(ethylenedithio)tetrathiafulvalene][8] and $(BETS)_2[Fe(tdas)_2]_2$ [BETS = bis(ethylenedithio)tetraselenafulvalene].[9] The structure of $(BEDT\text{-}TTF)_2[Fe(tdas)_2]$ contains conducting organic BEDT-TTF layers separated by dimerized $[Fe(tdas)_2]^{2-}$ anions, while the structure of $(BETS)_2[Fe(tdas)_2]_2$ is characterized by segregated columns of BETS dimers separated by columns of $Fe(tdas)_2$ dimers. In both salts, coexistence of conducting and magnetic properties was observed. The extended sulfur framework of BEDT-TTF, as compared to TTF, allows for increased side-to-side sulfur−sulfur interactions in the $(BEDT\text{-}TTF)_2[Fe(tdas)_2]$ salt leading to improved electrical conductivity: room-temperature conductivity for the BEDT-TTF salt is $\sim$1 S·cm^{-1} as compared to 0.03 S·cm^{-1} for the TTF analogue. Substitution of four of the eight sulfur atoms of BEDT-TTF with selenium leads to BETS, which favors the metallic state due to increased polarizabilities and orbital overlap between molecules induced by selenium atoms. Thus, while the TTF and BEDT-TTF derivatives exhibit semiconducting behavior, the BETS salt is metallic down to 200 K.

Analogous $Ni(tdas)_2$ salts have been less studied. A salt of composition $(TTF)_2[Ni(tdas)_2]$ has been prepared but not structurally characterized.[10] Its conducting properties seemed unrewarding (room-temperature conductivity on a compressed pellet was 10^{-1} S·cm^{-1} with an activation energy of 340 meV) when compared to $(TTF)[Ni(dmit)_2]$, which exhibits superconductivity under pressure (T_c = 1.62 K, 7 kbar).[11,12] Recently another salt, $(OMTTF)_2[Ni(tdas)_2]$[13] (OMTTF = octamethylenetetrathiafulvalene), has been obtained which is an insulator consisting of dimerized OMTTF radical cations and $[Ni(tdas)_2]^{2-}$ dianions. Attempts to prepare crystals of new charge transfer (CT) salts of other donors, including BEDT-TTF, with $[Ni(tdas)_2]^{2-}$ anions were reported to yield unsatisfactory results, although the reasons for these failures were not explained.[13]

The redox properties of $Ni(tdas)_2$ complexes have been reinvestigated and show, in contrast to what was previously reported,[10] the presence of a two-step redox process for the $[Ni(tdas)_2]$ dianion's oxidation.[13,14] Preliminary molecular orbital (MO) calculations on these systems were also performed showing the capability of the terminal sulfur atoms to promote intermolecular interactions.[14] This, in connection with the ability of the BEDT-TTF donor to form interlayer interactions in its 2D (super)conducting salts, prompted us to reinvestigate the complex formation of the paramagnetic $[Ni(tdas)_2]^-$ monoanion with BEDT-TTF. We report in this paper the synthesis, X-ray crystal structure, and physical properties of the $(BEDT\text{-}TTF)[Ni(tdas)_2]$ salt, the first crystallographically and magnetically characterized salt of an open-shell cation with the $Ni(tdas)_2^-$ monoanion that shows a packing pattern similar to that of the OMTTF salt in one of the layers but totally different physical properties.

Experimental Section

Synthesis of TBA[Ni(tdas)$_2$]. $(TBA)_2Ni(tdas)_2$ was prepared as previously described.[15] Iodine (0.15 g) in acetone (80 mL) was slowly added to $(TBA)_2Ni(tdas)_2$ (1.26 g) in the same solvent (120 mL), and the reaction mixture was stirred for 30 min under an argon atmosphere. Black needlelike crystals of $TBA[Ni(tdas)_2]$ were obtained by slow diffusion of diethyl ether into this solution at 0 °C (yield = 90%). Anal. Calcd for $C_{20}H_{36}N_5S_5Ni$: C, 42.48; H, 6.42; N, 12.38; S, 28.35. Found: C, 41.57; H, 6.92; N, 12.14; S, 29.16. IR (cm^{-1}): 2959 (m), 2872 (mw), 1470 (ms), 1404 (w), 1381 (mw), 1323 (m), 1236 (s), 1169 (w), 1064 (w), 1026 (w), 921 (w), 882 (mw), 820 (w), 784 (m), 770 (ms), 752 (mw), 735 (mw), 503 (w) and 490 (m). Raman (cm^{-1}): 2928 (m), 2869 (mw), 1443 (w), 1406 (w), 1322 (vs), 1244 (w), 1186 (w), 1149 (s), 764 (mw), 485 (mw), 385 (mw), 326 (mw), 267 (w) and 157 (s). Vibrational assignments have previously been made.[14]

Crystallization of (BEDT-TTF)[Ni(tdas)$_2$]. Prior to use, BEDT-TTF (Aldrich) was recrystallized from chloroform (Aldrich). The benzonitrile solvent (ACROS 99%) was degassed. Black platelike crystals of $(BEDT\text{-}TTF)[Ni(tdas)_2]$ were grown by using the previously described electrocrystallization technique.[16,17] The electrochemical H-cell was assembled in an argon-filled drybox. BEDT-TTF (10 mg) was dissolved in 5 mL of benzonitrile and placed in the anode chamber of the cell. $(TBA)[Ni(tdas)_2]$ (40 mg) was dissolved in 10 mL of benzonitrile and this solution divided between the anode and cathode compartments. A current density of 2.46 μA/cm^2 was applied. Crystallization of black crystals was observed on the anode surface within 1 day. Crystals were grown at 25 °C on platinum wire electrodes for a period of 43 days. IR (cm^{-1}): 2995 (vw), 1438 (mw), 1414 (ms), 1330(s), 1282 (m), 1017 (w), 888 (mw), 790 (m), 490 (s), 478 (ms) and 445 (m). Raman (cm^{-1}): 1580 (vw), 1400 (w), 1289 (mw), 1244 (s), 903 (w), 824 (w), 674 (w), 486 (s), 375 (mw), 337 (vs, ν_{Ni-S}), and 163 (ms).

Crystal Structure Determination. The structure of $(BEDT\text{-}TTF)[Ni(tdas)_2]$ was determined at 298 K by use of a Siemens

(7) Robertson, N.; Awaga, K.; Parsons, S.; Kobayashi, A.; Underhill, A. E. *Adv. Mater. Opt. Electron.* **1998**, *8*, 93.
(8) DePlano, P.; Leoni, L.; Mercuri, M. L.; Schlueter, J. A.; Geiser, U.; Wang, H. H.; Kini, A. M.; Manson, J. L.; Gómez-García, C. J.; Coronado, E.; Koo, H. J.; Whangbo, M. H. *J. Mater. Chem.* **2002**, *12*, 3570.
(9) Pilia, L.; Faulmann, C.; Mialfant, I.; Collière, V.; Mercuri, M. L.; DePlano, P.; Cassoux, P. *Acta Crystallogr. C* **2002**, *58*, 240.
(10) Hawkins, I.; Underhill, A. E. *J. Chem. Soc., Chem. Commun.* **1990**, 1593.
(11) Bousseau, M.; Valade, L.; Legros, J.-P.; Cassoux, P.; Garbauskas, M.; Interrante, L. V. *J. Am. Chem. Soc.* **1986**, *108*, 1908.
(12) Brossard, L.; Ribault, M.; Bousseau, M.; Valade, L.; Cassoux, P. *C. R. Acad. Sci., Ser. 2* **1986**, *302*, 205.
(13) Yamochi, H.; Sogoshi, N.; Simizu, Y.; Saito, G.; Matsumoto, K. *J. Mater. Chem.* **2001**, *11*, 2216.
(14) Deplano, P.; Marchio, L.; Mercuri, M. L.; Pilia, L.; Serpe, A.; Trogu, E. F. *Polyhedron* **2003**, *22*, 2175.
(15) Dyachenko, O. A.; Konovalikhin, S. V.; Kotov, A. I.; Shilov, G. V.; Yagubskii, E. B.; Faulmann, C.; Cassoux, P. *J. Chem. Soc., Chem. Commun.* **1993**, *1993*, 508.
(16) Emge, T. J.; Wang, H. H.; Beno, M. A.; Williams, J. M.; Whangbo, M. H.; Evain, M. *J. Am. Chem. Soc.* **1986**, *108*, 8215.
(17) Stephens, D. A.; Rehan, A. E.; Compton, S. J.; Barkhau, R. A.; Williams, J. M. *Inorg. Synth.* **1986**, *24*, 135.

Table 1. Summary of Crystallographic Data for (BEDT-TTF)[Ni(tdas)$_2$]

chem formula	$(C_{10}H_8S_8)Ni(C_2N_2S_3)_2$
fw	739.79
a, Å	17.2324(6)
b, Å	13.2740(5)
c, Å	10.9467(4)
α deg	90.00
β, deg	96.974(2)
γ, deg	90.00
V, Å^3	2485.5(2)
Z	4
space group	$P2_1/c$ (No. 14)
temp, K	295
λ, Å	0.710 73
ρ_{calcd}, g·cm^{-3}	1.977
μ, cm^{-1}	19.73
$R(F_o)^a$	0.0378 ($I > 2\sigma(I)$)
$R_w(F_o^2)^a$	0.0719 (all data)

^{a} $R(F_o) = \sum||F_o| - |F_c||/\sum|F_o|$, $R_w(F_o^2) = [\sum w(|F_o^2| - |F_c^2|)^2/\sum wF_o^2]^{1/2}$.

SMART single-crystal X-ray diffractometer equipped with a CCD-based area detector and a sealed-tube X-ray source. A summary of the crystallographic data is given in Table 1. Further details are available in the CIF file deposited as electronic Supporting Information. When the crystal was cooled to temperatures below 200 K, the peak widths of the X-ray reflections were significantly broadened.

Physical Properties. Variable-temperature susceptibility measurements were carried out in the temperature range 2−300 K at an applied magnetic field of 0.1 T on polycrystalline samples with a Quantum Design MPMS-XL-5 SQUID magnetometer. The sample was quickly cooled to 2 K (in less than 1/2 h), and then the measurement was done while warming the sample. The susceptibility data were corrected for the sample holder previously measured using the same conditions and from the diamagnetic contributions of the salt as deduced by using Pascal's constant tables.

Diffuse reflectance spectra (2000−300 nm) were recorded on KBr pellets with a Cary 5 spectrophotometer, equipped with a diffuse reflectance accessory. IR spectra (4000−350 cm^{-1}) were recorded in transmission through KBr pellets with a Bruker Equinox spectrometer. Raman spectra were recorded with a Bruker RFS100/S spectrometer fitted with a InGaAs detector (room temperature) and operating with a 1064 nm laser (Nd:YAG). The solid sample, as KBr powder, was introduced in a capillary tube and fitted into the compartment designed for a 180° scattering geometry; the power level of the laser source varied between 20 and 40 mW.

Dc conductivity measurements over the range 80−300 K were performed with the four contacts method in two different single crystals, giving reproducible results in both samples (below 80 K the resistivity of the crystals was too high to be measured). Contacts between the crystals and platinum wires (25 *μ*m diameter) were made using graphite paste. The samples were measured in a Quantum Design PPMS-9 with a dc current of 1 *μ*A. The cooling and warming rate was 2 K/min, and the results were, within experimental error, identical in the cooling and warming sweeps.

Band Structure Calculations. The tight-binding band structure calculations were done using an extended Hückel Hamiltonian[18] and a modified Wolfsberg−Helmholtz formula[19] to calculate the nondiagonal H_{ij} matrix elements. Double-ζ type orbitals for Ni 3d and single-ζ type for C 2s and 2p, S 3s and 3p, N 2s and 2p, H 1s, and Ni 4s and 4p were used. The exponents and parameters used in the calculations were taken from previous work.[20,21]

Results and Discussion

Crystal Structure. The atom numbering schemes used for the $[Ni(tdas)_2]^-$ anions and the BEDT-TTF electron-donor molecule are shown in Figure 1. There is one crystallographically unique BEDT-TTF molecule/unit cell. One of the ethylene end groups of the BEDT-TTF molecule is ordered, while the other is disordered (82% eclipsed/18% staggered with respect to the ordered group). Using the established empirical correlation between the C−S and C═C bond lengths and the donor charges in BEDT-TTF salts,[22] the oxidation state for the BEDT-TTF molecule in (BEDT-TTF)[Ni(tdas)$_2$] is estimated to be +1.0 (±0.1). This is in agreement with the +1 oxidation state expected from the stoichiometry.

As shown in Figure 2, (BEDT-TTF)[Ni(tdas)$_2$] crystallizes in a layered structure in which one layer contains dimerized $BEDT\text{-}TTF^+$ molecules and isolated $[Ni(tdas)_2]^-$ anions **A** whereas the other layer contains ribbons of $[Ni(tdas)_2]^-$ anions **B**. The unit cell contains one $[(BEDT\text{-}TTF)_2Ni(tdas)_2]^+$ layer and one $[Ni(tdas)_2]^-$ layer, which lie parallel to the *bc*-plane.

As shown in Figures 2 and 3, the BEDT-TTF molecules form dimerized units within the BEDT-TTF layer. However, no short S···S contacts exist between the BEDT-TTF molecules within these BEDT-TTF dimers. The distance between least-squares planes through the BEDT-TTF molecules of the dimers is 3.51(7) Å. The dimerized units are tilted 8.31(1)° with respect to each other. Several intralayer S···S contacts shorter than, or comparable to, the sum of the van der Waals radii exist between the BEDT-TTF molecules and the $[Ni(tdas)_2]^-$ anion **A**.

Both $[Ni(tdas)_2]^-$ anions lie on inversion centers and are essentially planar, with rms deviations of 0.0178 Å (molecule **A**) and 0.0415 Å (molecule **B**). For the $[Ni(tdas)_2]^-$ anion **A** the nickel atom deviates from the tdas plane by 0.044(1) Å, while for anion **B** the nickel atom is 0.110(2) Å out of the ligand plane. As shown in Figure 4, within the $[Ni(tdas)_2]^-$ anion layer, ribbons of $[Ni(tdas)_2]^-$ anions **B** are formed by 3.265(5) Å intermolecular contacts between the terminal sulfur atom, S23, of $[Ni(tdas)_2]^-$ (**B**) and N21. The dihedral angle between $[Ni(tdas)_2]^-$ **B** anions in adjacent chains is 35.71(5)°. The thermal ellipsoids for $[Ni(tdas)_2]^-$ **B** are notably larger than in $[Ni(tdas)_2]^-$ **A**. This is a result of the S···S contacts between the BEDT-TTF molecules and the $[Ni(tdas)_2]^-$ **A** anions which spatially confine this molecule more than the $[Ni(tdas)_2]^-$ **B** anions located in the anion layer. Likely, the enlarged displacement parameters in the latter are also related to the phase transition that causes the diffraction peaks to broaden between room temperature and

(18) Whangbo, H. H.; Hoffmann, R. *J. Am. Chem. Soc.* **1978**, *100*, 6093.
(19) Ammeter, J. H.; Bürgi, H. B.; Thibeault, J. C.; Hoffmann, R. *J. Am. Chem. Soc.* **1978**, *100*, 3686.
(20) Canadell, E.; Rachidi, I. E. I.; Ravy, S.; Pouget, J. P.; Brossard, L.; Legros, J. P. *J. Phys. (Paris)* **1989**, *50*, 2967.
(21) Veiros, L. F.; Calhorda, M. J.; Canadell, E. *Inorg. Chem.* **1994**, *33*, 4290.
(22) Guionneau, P.; Kepert, C. J.; Bravic, G.; Chasseau, D.; Truter, M. R.; Kurmoo, M.; Day, P. *Synth. Met.* **1997**, *86*, 1973−1974.

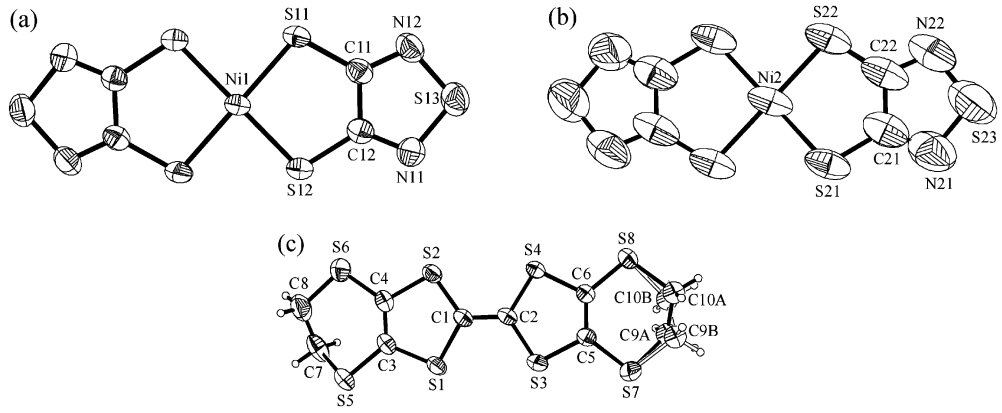

Figure 1. Labeling scheme of the two types of $[Ni(tdas)_2]^-$ anions (a) **A** and (b) **B** and (c) the BEDT-TTF molecule. Thermal ellipsoids are drawn at the 50% probability level. (The reason for the large thermal ellipsoids for **B** are discussed in the text.)

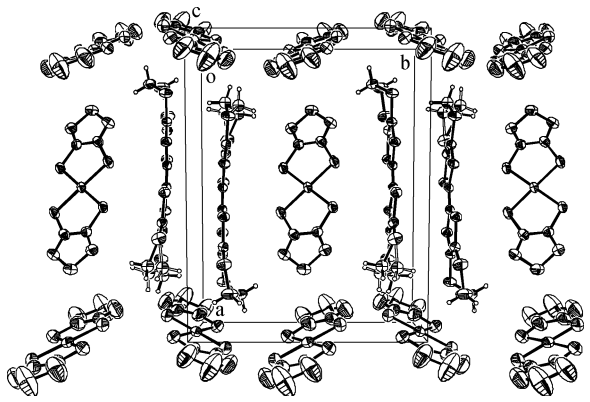

Figure 2. View of the alternating layers in the *bc*-plane. Thermal ellipsoids are drawn at the 50% probability level.

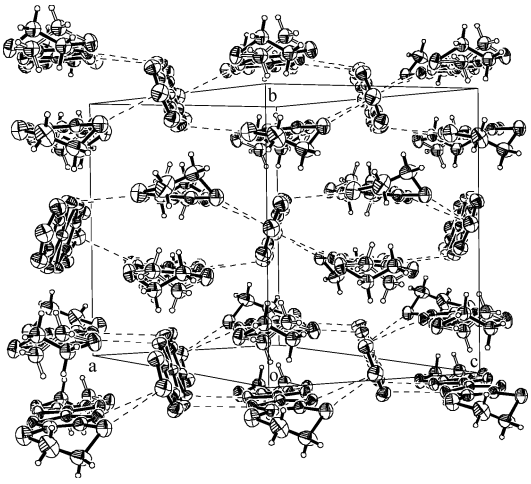

Figure 3. View of the mixed cation−anion layer showing the dimerized BEDT-TTF molecules and the isolated $[Ni(tdas)_2]^-$ **A** anions. Note that each $[Ni(tdas)_2]^-$ **A** anion is surrounded by six BEDT-TTF cations. Thermal ellipsoids are drawn at the 50% probability level. Dashed lines indicate the intermolecular contacts shorter than the sum of the van der Waals radii.

200 K. The Ni···S bond distances in $[Ni(tdas)_2]^-$ **A** are 2.1651(6) and 2.1681(6) Å, while in $[Ni(tdas)_2]^-$ **B** they are 2.170(1) and 2.182(1) Å. The other bond lengths of the two $[Ni(tdas)_2]^-$ anions (**A** and **B**) are quite similar.

Attempts to obtain the crystal structure at temperatures below the 200 K phase transition were unsuccessful due to a significant broadening of the diffraction peaks. However, the lattice distortion is reversible, as warming the crystal to room temperature restored the original diffraction profile.

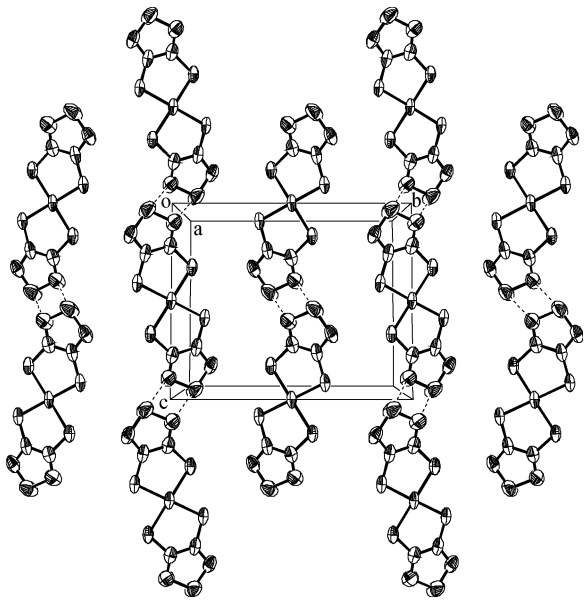

Figure 4. View of the $[Ni(tdas)_2]^-$ **B** anionic layer down the *a*-axis. Thermal ellipsoids are drawn at the 20% probability level. Dashed lines indicate the intermolecular contacts shorter than the sum of the van der Waals radii.

The crystal structure of (BEDT-TTF)$[Ni(tdas)_2]$ is related to that previously reported for $(OMTTF)_2[Ni(tdas)_2]$.[13] Both structures contain dimerized electron donor molecules separated by $[Ni(tdas)_2]^{n-}$ anions. The molecular planes of these anions are nearly perpendicular to the donor molecules. Both structures contain fully oxidized electron donor molecules. The $(OMTTF)_2[Ni(tdas)_2]$ structure contains $[Ni(tdas)_2]^{2-}$ dianions while (BEDT-TTF)$[Ni(tdas)_2]$ contains $[Ni(tdas)_2]^-$ monoanions. To balance charge, the (BEDT-TTF)$[Ni(tdas)_2]$ salt contains an additional layer of $[Ni(tdas)_2]^-$ anions separating the $(BEDT\text{-}TTF)_2[Ni(tdas)_2]$ layers. The $[Ni(tdas)_2]^-$ bond lengths in (BEDT-TTF)$[Ni(tdas)_2]$ are similar to those reported for $[Ni(tdas)_2]^{2-}$ in $(OMTTF)_2[Ni(tdas)_2]$. The largest deviations occur in the Ni−S bond lengths, which range from 2.165(1) to 2.182(1) Å for (BEDT-TTF)$[Ni(tdas)_2]$ while for $(OMTTF)_2[Ni(tdas)_2]$ are 2.196(13) and 2.193(14) Å.

Table 2. Average Bond Distances (in Å) in the Known $[Ni(tdas)_2]^{n-}$ ($n = 1$ or 2) Anions

compd	n	type	Ni−S	S−C	C−N	N−S	C−C	ref
(BEDT-TTF)[Ni(tdas)$_2$] **A**	−1	monomer	2.167	1.723	1.321	1.639	1.434	this work
(BEDT-TTF)[Ni(tdas)$_2$] **B**	−1	monomer	2.176	1.714	1.315	1.627	1.438	this work
(PBu_4)[Ni(tdas)$_2$]	−1	dimer	2.22	unavailable				23
$OMTTF_2$[Ni(tdas)$_2$]	−2	monomer	2.195	1.733	1.321	1.648	1.435	13
$(TBA)_2$[Ni(tdas)$_2$]	−2	monomer	2.209	1.714	1.314	1.644	1.464	15
$(TEA)_2$[Ni(tdas)$_2$]	−2	monomer	2.200	1.724	1.323	1.650	1.438	15

Only three other structures of the $[Ni(tdas)_2]^{n-}$ anion have been reported. (PBu_4)[Ni(tdas)$_2$] (Bu = *n*-butyl, C_4H_9) contains dimerized $[Ni(tdas)_2]^-$ monoanions,[23] while the $(TEA)_2$[Ni(tdas)$_2$] (TEA = tetraethylammonium) and $(TBA)_2$-[Ni(tdas)$_2$] salts contain discrete $[Ni(tdas)_2]^{2-}$ dianions.[15] As shown in Table 2, the Ni−S bond lengths in the PBu_4^+ salt (for the sulfur atoms not involved in the intradimer interactions) are 2.22 Å, while they are slightly shorter in the dianions: 2.200(1) and 2.209(3) Å for $(TEA)_2$[Ni(tdas)$_2$] and $(TBA)_2$[Ni(tdas)$_2$], respectively.

Magnetic Properties. As illustrated in Figure 5, the thermal dependence of the product of the molar magnetic susceptibility with the temperature ($\chi_m T$) of the title compound shows, at room temperature, a value of 0.41 emu·K·mol^{-1}. This value remains constant when the temperature is decreased to approximately 50 K. Below this temperature the $\chi_m T$ shows a smooth continuous decrease to reach a value of 0.25 emu·K·mol^{-1} at 2 K. This behavior indicates that (BEDT-TTF)[Ni(tdas)$_2$] is a $S = 1/2$ paramagnet that exhibits a weak antiferromagnetic coupling (as indicated by the smooth decrease of the $\chi_m T$ product at low temperatures).

The question now is the following: where is the one unpaired electron/formula unit located? If we assume that the charge on the BEDT-TTF molecules is not +2 but rather +1, as deduced from the bond lengths (see above), then the unpaired spin can be either on the $[Ni(tdas)_2]^-$ anions or on the $BEDT\text{-}TTF^+$ cations. Since the structural data as well as the electronic and vibrational spectroscopic results (see below) indicate that on one hand the BEDT-TTF molecules are strongly dimerized and probably strongly antiferromagnetically coupled and on the other hand the $[Ni(tdas)_2]^-$ anions are quite well isolated, we can conclude that the unpaired electron lies on the $[Ni(tdas)_2]^-$ anions and, therefore, the $BEDT\text{-}TTF^+$ radicals do not contribute to the magnetic moment of the title compound. Nevertheless, the definite proof is provided by the EPR spectrum (see below).

From the structural data we can assume that the $[Ni(tdas)_2]^-$ **A** anions (those in the BEDT-TTF layer) must be isolated from the magnetic point of view whereas the $[Ni(tdas)_2]^-$ **B** anions may present some antiferromagnetic interactions that account for the decrease in the $\chi_m T$ product at low temperatures. Accordingly, we have fitted the susceptibility data to a regular $S = 1/2$ antiferromagnetic chain (formed by the **B**-type anions) plus a monomeric contribution coming from the **A**-type anions. We have assumed that the *g*-value of both anions is the same to reduce the number of adjustable parameters. As indicated by the solid line in Figure 5, this model reproduces very satisfactorily the magnetic properties in the whole temperature range with the following set of parameters: $g = 2.090(2)$; $J = -2.52(4)$ cm^{-1}. The weak antiferromagnetic intermolecular coupling between the **B**-type $[Ni(tdas)_2]^-$ units suggests that although small, there is a nonnegligible interaction between these anions, in agreement with the presence of short interanion S−N distances observed in the crystal structure (see above).

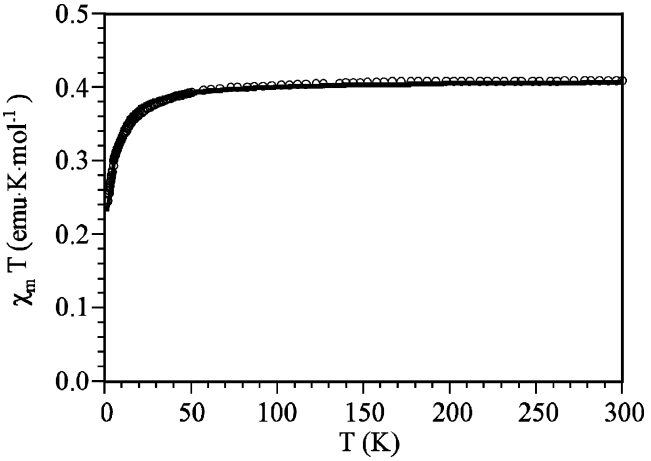

Figure 5. Thermal variation of the product of the molar magnetic susceptibility times the temperature ($\chi_m T$). The solid line represents the best fit to the model (see text).

It is interesting to note that the behavior of the $[Ni(tdas)_2]^-$ anion in the title compound is very different from that observed in the salt (TBA)[Ni(tdas)$_2$], where the anions are strongly antiferromagnetically coupled, giving an almost diamagnetic behavior, even at room temperature, and a very weak EPR signal coming from isolated monomeric impurities.[24]

As illustrated in Figure 6a, the X-band EPR spectrum at room temperature of a polycrystalline sample of the title compound shows an anisotropic signal with a main feature at 3417 G ($g = 2.060$) and a peak at lower fields (3160 G, $g = 2.228$). The Q-band spectrum of the same sample at room temperature, shown in Figure 6b, allows a better resolution of the main signal splitting it into two signals located at 11723 and 11877 G ($g = 2.080$ and 2.053, respectively). Furthermore, up to four shoulders can be observed in the signal at $g = 2.080$ corresponding to a hyperfine coupling of approximately 100 G. This spectrum,

(23) Schenk, S.; Hawkins, I.; Wilkes, S. B.; Underhill, A. E.; Kobayashi, A.; Kobayashi, H. *J. Chem. Soc., Chem. Commun.* **1993**, 1648.

(24) The magnetic susceptibility of (TBA)[Ni(tdas)$_2$] (in the 20−400 K range) can be satisfactorily reproduced with a $S = 1/2$ dimer model with $g = 2$ (fixed value), a strong antiferromagnetic coupling constant, $J = -509(1)$ cm^{-1}, and a small monomeric impurity of 4%. This small monomeric impurity can also be observed in the room-temperature EPR spectrum of this salt that shows a very weak anisotropic signal at $g = 2.054$ with a peak at $g = 2.190$. This signal is identical (although much more weaker) to that observed in the title compound (coming from the monomeric $[Ni(tdas)_2]^-$ anion).

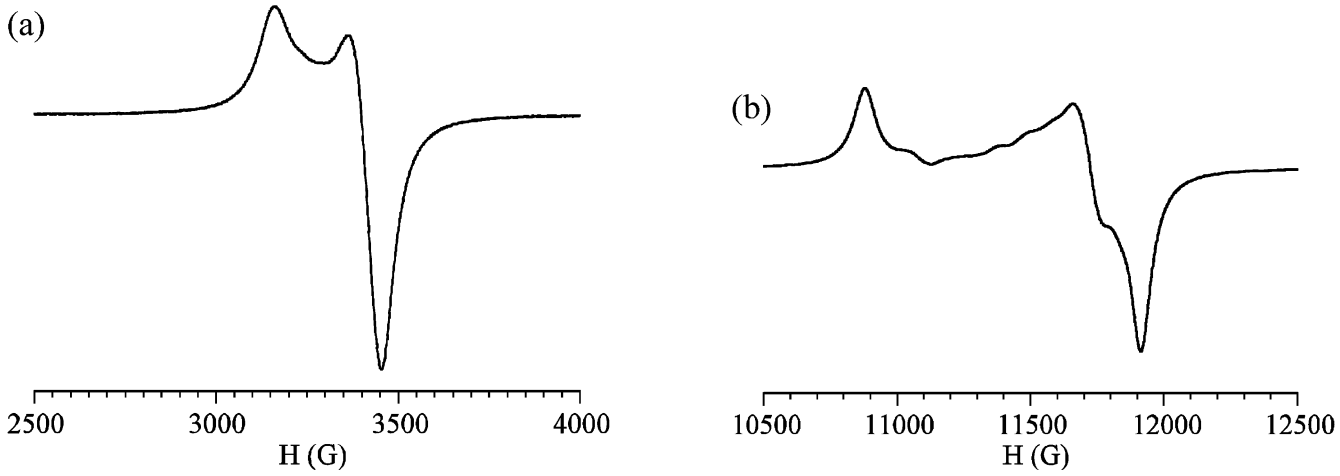

Figure 6. EPR spectra at room temperature of a polycrystalline sample of the title compound in (a) X- and (b) Q-bands.

including the hyperfine structure, is very similar to that obtained in other nickel bis(dithiolene) complexes.[25] The observed hyperfine structure originates from the coupling of the unpaired electon in the $[Ni(tdas)_2]^-$ unit and the ^{61}Ni nucleus ($I = 3/2$, natural abundance 1.13%) and confirms the considerable metal contribution to the SOMO of the complex. Besides this anisotropic line, a very narrow ($\Delta H \approx 4$ G) and weak feature located at 3380−3381 G ($g = 2.0011-2.0018$) can be observed in the X-band spectra of some single crystals. The low anisotropy and ΔH values, together with the position and weakness of this signal, indicate that it arises from a small amount of isolated BEDT-TTF^+ radicals which is attributed to the presence of crystal defects.[13,26,27]

The high anisotropy and *g*-value of the EPR signal together with the resemblance between this EPR spectrum and those observed in other nickel bis(dithiolene) complexes (where similar *g*-values and hyperfine splitting have been observed)[25] suggest that this EPR feature must be attributed to the anisotropic planar $[Ni(tdas)_2]^-$ anions, confirming the susceptibility data that indicate the presence of one unpaired electron in the $[Ni(tdas)_2]^-$ units (see above). Thus, both experiments (the EPR and the susceptibility data) indicate that the charge on the $[Ni(tdas)_2]$ unit is −1 rather than −2, supporting the charge assignment of +1 made from the bond distances in the BEDT-TTF molecules (see above).

The anisotropy of the EPR signal can be better observed in the angular variation of the X-band EPR spectrum of a single crystal of the title compound. As shown in Figure 7, these spectra show an isotropic single line with a line width (ΔH) of 50−65 G whose position varies from 3035 to ca. 3300 G ($g = 2.23-2.05$). As expected, the sum of all the spectra (taken every 5° rotation) shows a spectrum very similar to that obtained with the polycrystalline sample (Figure 6a). Note that from the structural data, in principle,

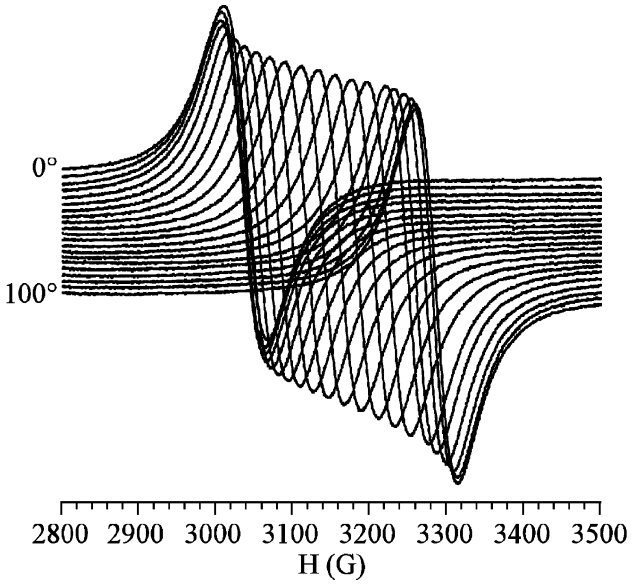

Figure 7. Angular dependence of the X-band EPR spectrum of a single crystal of the title compound. The angle refers to the orientation of the magnetic field with respect to the crystal's *bc*-plane (the best developed face of the single crystals).

there should be four EPR lines since there are two different orientations for each $[Ni(tdas)_2]^-$ anion. Nevertheless, the presence of a weak interaction among them (as confirmed by the magnetic data and the band structure calculation, see below) produces an exchange narrowing of the four signals resulting in a symmetrical anisotropic signal which is the average of the four symmetrical anisotropic signals from the anions.

The thermal variation of the Q-band EPR spectrum of the title compound confirms the paramagnetic behavior of the anisotropic signal from the $[Ni(tdas)_2]^-$ anions and also shows a decrease of the magnetic moment at low temperatures, in agreement with the static susceptibility data. Moreover, the temperature dependence also confirms that the weak signal at $g \approx 2$, attributed to a small amount of isolated BEDT-TTF^+ molecules, remains negligible compared to the main signal from the $[Ni(tdas)_2]^-$ anions.

As this is the first known example of isolated $[Ni(tdas)_2]^-$ anions, we cannot compare these magnetic results with other

(25) Sellmann, D.; Binder, H.; Haussinger, D.; Heinemann, F. W.; Sutter, J. *Inorg. Chim. Acta* **2000**, *300*−*302*, 829.
(26) Gómez-García, C. J.; Giménez-Saiz, C.; Triki, S.; Coronado, E.; Le Magueres, P.; Ouahab, L.; Ducasse, L.; Sourisseau, C.; Delhaes, P. *Inorg. Chem.* **1995**, *34*, 4139.
(27) Coronado, E.; Galán-Mascarós, J. R.; Giménez-Saiz, C.; Gómez-García, C. J.; Triki, S. *J. Am. Chem. Soc.* **1998**, *120*, 4671.

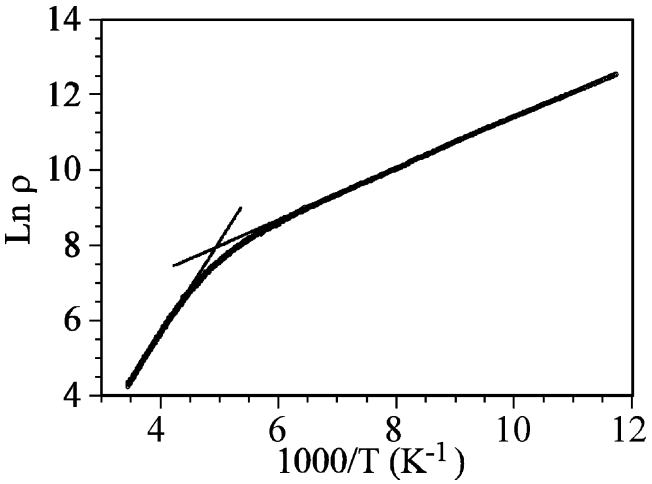

Figure 8. Plot of the logarithm of the dc electrical resistivity of the title compound as a function of reciprocal temperature showing the two semiconducting regimes and the transition between them at approximately 200 K.

known examples. Nevertheless, very recently some of us have found that the $[Ni(tdase)_2]^-$ (tdase = 1,2,5-thiadiazole-3,4-diselenolate) monoanion, formed with the closely related selenium-containing tdase^{2-} ligand (mixed $S_{0.6}/Se_{0.4}$ occupancy of the thiolic chalcogen atoms in the 1,2,5-thiadiazole-3,4-dithiolate ligand), shows in solution a similar EPR signal[14] with a line width of approximately 60 G and a *g* value of 2.15.[28]

Electrical Properties. As shown in Figure 8, the dc electrical conductivity of the title compound shows a room-temperature conductivity of 0.018 S·cm^{-1} and two semiconducting regimes with activation energies of 58 and 212 meV above and below the transition temperature (≈200 K), respectively. This reversible semiconducting-to-semiconducting transition has already been observed in other radical salts at similar temperatures and has been attributed to an ordering of the ethylene group of the ET donor.[29] This ordering of the ethylene group may induce small structural changes in the conducting sublattice and, therefore, in its conducting properties. This transition is likely related to the observed broadening of the peak widths of the X-ray reflections taking place around 200 K.

Diffuse Reflectance and Vibrational Spectroscopy. The reflectance spectrum of (BEDT-TTF)[Ni(tdas)$_2$] has been deposited as Supporting Information. The first band at ∼6600 cm^{-1} is ascribable to the intradimer transition of the BEDT-TTF radical cations while the second band at ∼10 600 cm^{-1} (D band) is due to an intramolecular transition of the BEDT-TTF$^+$ radical cation. This band partially overlaps the typical peak of the $[Ni(tdas)_2]^-$ monoanion at ∼11200 cm^{-1}. No band below 5000 cm^{-1}, which is present in mixed-valence BEDT-TTF salts, is observed. These features are in accordance with structural and magnetic results showing that the BEDT-TTF molecules in the dimers bear an integer oxidation state (+1). The reflectance spectra have been proposed by Saito et al.[13,30] as an optical probe for identifying the charge in BEDT-TTF-based donor radical salts even more effective than the widely used bond-length analysis. Further evidence for the presence of $(BEDT\text{-}TTF)_2^{2+}$ dimers comes from the inspection of the infrared spectrum (deposited as Supporting Information) where peaks at 1414 (ν_2), 1330 (ν_3), 490 (ν_9), and 478 (ν_{10}) cm^{-1}, assigned to the a_g vibration modes, appear as a consequence of the dimerization of the cation.[13,30]

Electronic Structure. Tight-binding band structure calculations were carried out for both the complete 3D lattice and the separate $[Ni(tdas)_2]$ and BEDT-TTF sublattices. The BEDT-TTF dimers have a very substantial energy difference between the bonding and antibonding combination of the HOMOs ($\Delta = 0.30$ eV), every one of these levels leading to nondispersive bands. This energy gap clearly shows that the dimers must be considered as $(BEDT\text{-}TTF)_2^{2+}$ in agreement with the structural and EPR data. In nickel bis-(dithiolene)-based molecular conductors both the HOMO and LUMO can play an important role in the electronic structure[31−33] as far as the HOMO−LUMO gap is of the order of 0.40 eV according to single-ζ extended Hückel calculations. Here, the gaps are calculated to be 0.36 and 0.35 eV for $[Ni(tdas)_2]^-$ **A** and **B**, respectively. However, the tight-binding calculations show that the interactions in the solid are small enough to keep the HOMO and LUMO bands well separated and without a noticeable mixing so that the HOMO levels are completely filled.

Whereas the interaction between the BEDT-TTF and $Ni(tdas)_2$ sublattices was found to be small, the two different types of $[Ni(tdas)_2]^-$ anions do exhibit some interaction. Shown in Figure 9a are the LUMO bands calculated for the $Ni(tdas)_2$ sublattice. There are four $[Ni(tdas)_2]^-$ units (two of type **A** and two of type **B**) per unit cell and thus four mainly LUMO bands. The upper pair of bands is primarily built from the LUMO of $[Ni(tdas)_2]^-$ **B** whereas the lower pair is mostly built from the LUMO of $[Ni(tdas)_2]^-$ **A**. The existence of $(BEDT\text{-}TTF)_2^{2+}$ units means that the bands in Figure 9a must be filled with four electrons. However, the lower pair of bands cannot be doubly filled. According to its nature such filling would mean that the $[Ni(tdas)_2]^-$ **A** would formally have a charge of 2$^-$, and consequently, $[Ni(tdas)_2]^-$ **B** would be formally neutral, in contradiction with the structural and EPR results. Therefore, every pair of bands of Figure 9a must split into two pairs of Mott−Hubbard subbands as a result of electron repulsions (*U*) in such a way that one of the pairs of LUMO subbands associated with both $[Ni(tdas)_2]^-$ **A** and **B** is filled and the other

(28) Note that these values correspond to the average *H* and *g* values observed in the title compound and that the only difference between both spectra is that the signal of the $[Ni(tdase)_2]^-$ monoanion is isotropic since the spectrum was recorded in solution, where the anions are present as isolated monomers.

(29) Tanatar, M. A.; Kagoshima, S.; Ishiguro, T.; Ito, H.; Yefanov, V. S.; Bondarenko, V. A.; Kushch, N. D.; Yagubskii, E. B. *Phys. Rev. B* **2000**, *62*, 15561.

(30) Saito, G.; Izukashi, H.; Shibata, M.; Yoshida, K.; Kushch, L. A.; Kondo, T.; Yamochi, H.; Drozdova, O. O.; Matsumoto, K.; Kusunoki, M.; Sakaguchi, K.; Kojima, N.; Yagubskii, E. B. *J. Mater. Chem.* **2000**, *10*, 893.

(31) Canadell, E.; Ravy, S.; Pouget, J. P.; Brossard, L. *Solid State Commun.* **1990**, *75*, 633.

(32) Canadell, E. *New J. Chem.* **1997**, *21*, 1147.

(33) Rovira, C.; Novoa, J. J.; Mozos, J. L.; Ordejon, P.; Canadell, E. *Phys. Rev. B* **2002**, *65*, 081104.

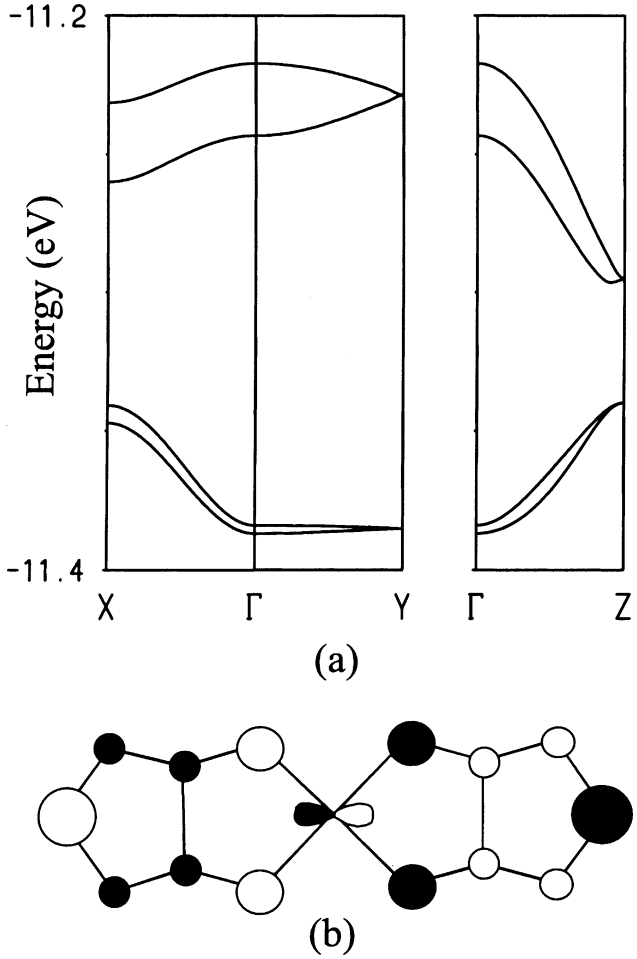

Figure 9. (a) Calculated band structure for the $Ni(tdas)_2$ sublattice of (BEDT-TTF)[$Ni(tdas)_2$], where $\Gamma = (0, 0, 0)$, $X = (a^*/2, 0, 0)$, $Y = (0, b^*/2, 0)$, and $Z = (0, 0, c^*/2)$. (b) Schematic representation (top view) of the LUMO of $Ni(tdas)_2$.

is empty. In other words, there is an electron localization [i.e., one electron/$Ni(tdas)_2$ site] due to the electron repulsions so that (BEDT-TTF)[$Ni(tdas)_2$] is a Mott−Hubbard semiconductor.

Although relatively small, as corresponds to a localized system, both pairs of bands exhibit some dispersion, evidencing the existence of interactions between the localized electrons. Let us note that, as is usual in extended Hückel calculations for transition metal based systems, we have used a single-ζ basis set for the nontransition metal atoms and, consequently, the dispersions are expected to be somewhat underestimated. As shown in Figure 9b, the LUMO of $Ni(tdas)_2$ has the larger contribution from the terminal sulfur atoms. It is because of the existence of relatively short contacts in which these sulfur atoms are implicated that the bands of Figure 9a acquire dispersion along the *c* and *a* directions. The important contacts are those among the terminal sulfur atoms (S23) of $[Ni(tdas)_2]^-$ **B** and the nitrogen N21 atoms of adjacent **B** type anions along *c* (S23···N21: 3.265 Å) as well as those with the terminal sulfur atoms of type **A** (S13) (S23···S13: 3.933 Å). Although the latter may seem somewhat long, note that both sulfur atoms are terminal (and thus contribute with large coefficients to the LUMO) and that the orientation is appropriate for quite good σ-type overlap. It is through these interactions that the localized electrons of the $[Ni(tdas)_2]^-$ anions communicate. The conductivity of this kind of localized systems is influenced by both the existence of $Ni(tdas)_2\cdots Ni(tdas)_2$ interactions and the magnitude of the intrasite electron repulsions (U). Since U is essentially immune to small structural changes, the conductivity change near 200 K is most likely due to some structural change, probably an ordering of the ethylene groups of the BEDT-TTF donors which induce changes in the $Ni(tdas)_2$ sublattice decreasing the above-mentioned short intermolecular contacts.

Conclusions

The title compound represents the first example of a monomeric $[Ni(tdas)_2]^-$ monoanion and has allowed the study, for the first time, of the magnetic behavior of such a monoanion. This study indicates that (BEDT-TTF)[$Ni(tdas)_2$] is an $S = 1/2$ paramagnet with the unpaired electron located in the isolated $[Ni(tdas)_2]^-$ monoanions presenting weak antiferromagnetic interanion interactions. The BEDT-TTF sublattice does not contribute to the magnetic properties as it consists of strongly antiferromagnetically coupled $(BEDT\text{-}TTF)_2^{2+}$ dimers as shown by the EPR spectra, magnetic susceptibility measurements, diffuse reflectance, and vibrational spectroscopy. The electrical conductivity of this salt shows a semiconductor−semiconductor transition at about 200 K that may be attributed to an ordering of the disordered terminal ethylene group of the BEDT-TTF molecule. This fact may also be the origin of the broadening of the peak widths of the X-ray reflections observed below 200 K.

Acknowledgment. This work has been developed in the framework of a European COST action (Inorganic Molecular Conductors), an INTAS project (Grant 0651) and an Italian-Spanish Integrated Action (Grant HI-0076). Work at the Institute of Molecular Science of the University of Valencia is supported by the Spanish Ministerio de Ciencia y Tecnología (Grant MAT2001-3507-C02-01). Work at Argonne National Laboratory is supported by the US-DOE under Contract W-31-109-ENG-38. Work at the Institut de Ciència de Materials de Barcelona is supported by the DGI-Spain (Project BFM2000-1312-C02-01) and Generalitat de Catalunya (Project 2001 SGR 333).

Supporting Information Available: Crystallographic data in CIF format, a UV−vis−NIR spectrum of (BEDT-TTF)[$Ni(tdas)_2$] in a KBr, and an IR spectrum of (BEDT-TTF)[$Ni(tdas)_2$] in a KBr pellet. This material is available free of charge via the Internet at http://pubs.acs.org.

IC035079Y